Since January 2020 Elsevier has created a COVID-19 resource centre with free information in English and Mandarin on the novel coronavirus COVID-19. The COVID-19 resource centre is hosted on Elsevier Connect, the company's public news and information website.

Environmental Pollution 267 (2020) 115617

Contents lists available at ScienceDirect

Environmental Pollution

journal homepage: www.elsevier.com/locate/envpol

Air pollution episodes during the COVID-19 outbreak in the Beijing–Tianjin–Hebei region of China: An insight into the transport pathways and source distribution☆

Na Zhao [a], Gang Wang [b, *], Guohao Li [c, d], Jianlei Lang [e, **], Hanyu Zhang [e]

[a] Shanghai Key Laboratory of Atmospheric Particle Pollution and Prevention, Department of Environmental Science and Engineering, Institute of Atmospheric Sciences, Fudan University, Shanghai, 200433, China
[b] Department of Environmental and Safety Engineering, College of Chemical Engineering, China University of Petroleum (East China), Qingdao, 266580, China
[c] Municipal Research Institute of Environmental Protection, Beijing, 100037, China
[d] Key Laboratory of Beijing on VOC Pollution Control Technology and Application of Urban Atmosphere, Beijing, 100037, China
[e] Key Laboratory of Beijing on Regional Air Pollution Control, Beijing University of Technology, Beijing, 100124, China

ARTICLE INFO

Article history:
Received 29 July 2020
Received in revised form
19 August 2020
Accepted 5 September 2020
Available online 8 September 2020

Keywords:
Air pollution
Beijing–Tianjin–Hebei region
COVID-19
Regional transport
PSCF/CWT

ABSTRACT

Although anthropogenic emissions decreased, polluted days still occurred in the Beijing–Tianjin–Hebei (BTH) region during the initial outbreak of the coronavirus disease (COVID-19). Analysis of the characteristics and source distribution of large-scale air pollution episodes during the COVID-19 outbreak (from 23 January to April 8, 2020) in the BTH region is helpful for exploring the efficacy of control measures and policy making. The results indicated that the BTH region suffered two large-scale air pollution episodes (23–28 January and 8–13 February), which were characterized by elevated $PM_{2.5}$, SO_2, NO_2, and CO concentrations, while the O_3 concentration decreased by 1.5%–33.9% (except in Shijiazhuang, where it increased by 16.6% during the second episode). These large-scale air pollution episodes were dominated by unfavorable meteorological conditions comprising a low wind speed and increased relative humidity. The transport pathways and source distribution were explored using the Hybrid Single Particle Lagrangian Integrated Trajectory (HYSPLIT), potential source contribution function (PSCF), and concentration weighted trajectory (CWT) models. The air pollution in the BTH region was mainly affected by local emission sources during the first episode, which contributed 51.6%–60.6% of the total trajectories in the BTH region with a $PM_{2.5}$ concentration ranging from 146.2 μg/m^3 to 196.7 μg/m^3. The short-distance air masses from the southern and southwestern areas of the BTH region were the main transport pathways of airflow arriving in the BTH region during the second episode. These contributed 51.9%–57.9% of the total trajectories and originated in Hebei, Henan, central Shanxi, and Shaanxi provinces, which were the areas contributing the most to the $PM_{2.5}$ level and exhibited the highest PSCF and CWT values. Therefore, on the basis of local emission reduction, enhancing regional environmental cooperation and implementing a united prevention and control of air pollution are effective mitigation measures for the BTH region.

1. Introduction

The coronavirus disease (COVID-19) broke out worldwide in the first half of 2020 and became a global public health threat. Unconventional and stringent prevention and control measures were implemented by many countries and cities to prevent the further spread of the virus. In China, preventive lockdown was first implemented on January 23, 2020 in Wuhan, Hubei Province, and was subsequently followed by other provinces and cities (Le et al., 2020). Through a joint national effort, the lockdown was gradually lifted, with Wuhan being the last city in China to be removed from lockdown on April 8, 2020.

Overall, the air quality in China improved during the COVID-19

☆ This paper has been recommended for acceptance by Da Chen.

* Corresponding author.
** Corresponding author.
E-mail addresses: wangg@upc.edu.cn (G. Wang), jllang@bjut.edu.cn (J. Lang).

https://doi.org/10.1016/j.envpol.2020.115617
0269-7491/

outbreak as a result of reduced anthropogenic emissions (Zheng et al., 2020; Faridi et al., 2020; Chu et al., 2020; Navinya et al., 2020; Xu et al., 2020). The concentrations of particulate matter ($PM_{2.5}$ and PM_{10}, i.e., aerodynamic diameter of <2.5 μm and 10 μm, respectively), SO_2, NO_2, and CO decreased in comparison to 2017–2019 in 366 urban areas across mainland China, while the O_3 concentration increased (Chen et al., 2020b). However, large-scale air pollution episodes still occurred, with the daily average concentration of $PM_{2.5}$ exceeding 200 μg/m^3 due to unfavorable meteorological conditions in northern China during the COVID-19 (Le et al., 2020; Wang et al., 2020; Zhang et al., 2020b).

The regional transport of pollutants plays a critical role in the variation of air quality. The Hybrid Single Particle Lagrangian Integrated Trajectory (HYSPLIT), potential source contribution function (PSCF), and concentration weighted trajectory (CWT) models have been extensively applied to investigate the regional transport pathways of air masses and source distribution during summer, winter, and pollution episodes (Ding et al., 2017; Li et al., 2017b; Hui et al., 2019; Xiong and Du, 2020). Studies have investigated the pollution source distributions corresponding to the Summer Olympic Games, Asia-Pacific Economic Cooperation (APEC), and Grand Military Parade held in August 2008, November 2014, and September 2015, respectively, in Beijing (Liu et al., 2016; Qiao et al., 2017). Unconventional and stringent emission reduction measures were also implemented by Chinese government to achieve "Olympic blue", "APEC blue", and "Parade blue". The emission reduction rates for SO_2, NO_x, volatile organic compounds (VOCs), and $PM_{2.5}$ in Beijing during these events were 35%–41%, 44%–51%, 30%–57%, and 37%–42%, respectively (no value for $PM_{2.5}$ during the 2008 Olympics) (Wang et al., 2010, 2017). However, the meteorological conditions and pollutant emissions during the COVID-19 outbreak were different from these three earlier events or other studied periods. Firstly, the previous three events were held during the summer and autumn in Beijing when no air pollution episodes occurred. The regional transport pathways of air masses may be influenced by the local climate in different seasons (Wang et al., 2015b). Secondly, the potential source regions may be influenced by the emission distribution. In the case of the COVID-19 lockdown period, there was a larger impact scope and a longer impact time with a significant emission reduction compared with previous three earlier events. Chen et al. (2020b) reported that nationwide contingency plans were implemented to shut down traffic and public activities in China, and that almost everyone was isolated at home during the COVID-19.

The Beijing–Tianjin–Hebei (BTH) region is the largest economic core area in northern China; it has highest level of development and generated 8.5% of the total national gross domestic product (GDP) in 2019 (http://data.stats.gov.cn/index.htm). The BTH region has experienced rapid economic development, industrialization, and urbanization over the last few decades (Lang et al., 2012; Wang et al., 2015a). Although the air quality in the BTH region has improved significantly since the implementation of the "Action Plan for Prevention and Control of Air Pollution" in September 2013 (Geng et al., 2019; Wang et al., 2019), 16 of the 20 most polluted cities are located in the BTH region according to the 2019 air quality status reports of 168 cities in China (MEE, 2020).

The COVID-19 lockdown in China provided an excellent opportunity to investigate the corresponding air pollution characteristics and source distribution in the BTH region. To provide a sound basis for the effective control of urban agglomerated air pollution, it is of great importance to investigate the transport pathways and potential source regions during air pollution episodes. This study analyzed the air quality during the COVID-19 outbreak (from 23 January to April 8, 2020) and characteristics of large-scale air pollution episodes in the BTH region. Backward trajectory, PSCF, and CWT analyses were conducted to explore the transport pathways and potential source regions of air pollutants during pollution episodes. The results can help to guide future control strategies and policy making in the BTH region.

2. Methods

2.1. Data source

In this study, Beijing, Tianjin, and Shijiazhuang were selected to analysis the air quality and pollution episodes in the BTH region. Beijing, as the capital of China, is the center of politics, economics, and culture. Tianjin is one of the four directly governed municipalities of China. Shijiazhuang, as the capital of Hebei Province, is an important industrial city in the BTH region. The hourly concentrations of $PM_{2.5}$, SO_2, NO_2, O_3, and CO from 35 monitoring stations in Beijing, Tianjin, and Shijiazhuang were obtained from China's National Environmental Monitoring Centre for the period from 23 January to April 8, 2020. The standard procedure (e.g., monitoring system, analysis method, quality assurance, and quality control) for monitoring of pollutants are illustrated in the Text S1. Additionally, hourly meteorological data including wind speed, relative humidity, and visibility for Beijing, Tianjin, and Shijiazhuang were collected from the Meteorological Information Comprehensive Analysis and Process System (MICAPS) of the Chinese Meteorological Administration. Fig. S1 illustrates the location of the BTH region and the monitoring stations of air quality and meteorology. Under normal conditions, 1848 sets of data can be collected for each of the three cities. However, 1839–1840 and 1741–1746 sets of valid data were obtained for concentration and meteorological, respectively for the three cities. The detailed information of number of valid data are displayed in Table S2. In case the missing data occurred, the data were omitted in this study.

2.2. Model

2.2.1. HYSPLIT

The air-mass backward trajectories were calculated and clustered to track the transport pathways of airflow arriving in Beijing (39.914° N, 116.405° E), Tianjin (39.117° N, 117.179° E), and Shijiazhuang (38.050° N, 114.493° E) using the HYSPLIT model. The 72-h backward trajectories started every hour (0:00–23:00) each day and were calculated at 50, 100, and 500 m above ground level (AGL) using meteorological data (Global Data Assimilation System, ftp://arlftp.arlhq.noaa.gov/pub/archives/gdas1/) during the air pollution episodes. Therefore, a total of 72 trajectories per day were obtained for each of the three cities (Beijing, Tianjin, and Shijiazhuang). A trajectory cluster analysis was also conducted to divide the abundant trajectories into distinct clusters using the TrajStat model (version 1.2.2.6).

2.2.2. PSCF

The PSCF is a conditional probability function that can be applied to identify potential source regions of air pollution because backward trajectory analysis can only give the air-mass transport pathways. Prior to performing the PSCF analysis in this study, the geographic region covered by the trajectories was divided into an array of 0.5 ° × 0.5 ° grid cells. The PSCF is defined as $PSCF_{ij} = m_{ij}/n_{ij}$, where n_{ij} and m_{ij} represent the number of all trajectories and pollution trajectories through the grid cells, respectively (John et al., 2012). Grid cells with higher PSCF values indicate that the corresponding region is a potential source region of severe pollution. The daily $PM_{2.5}$ concentration higher than 150 μg/m^3 refers to heavily polluted day based on the Technical Regulation on Ambient Air Quality Index (on trial; HJ633-2012). Therefore, we set the

reference value of $PM_{2.5}$ concentration as 150 μg/m^3 in this study. Pollution trajectories represent the trajectories with pollution values that exceed this value. To reduce the influence of small values of n_{ij}, an arbitrary weight function, W_{ij}, was multiplied by the PSCF value to eliminate the uncertainty of small values, where $WPSCF = W_{ij} \times PSCF_{ij}$ (Cheng et al., 1993). High WPSCF values indicate higher probabilities of grid cells being potential source regions that contribute to air pollution in the target city.

2.2.3. CWT

The WPSCF analysis can only reflect the proportion of polluted trajectories in a cell grid and cannot distinguish the contributions of those cell grids with the same WPSCF values as the receptor sites. Therefore, the CWT analysis was further applied to calculate the relative contribution of different source areas, in which a residence-time weighed concentration was assigned to each grid cell by averaging each pollutant mass concentration with a trajectory associated with the grid cell. The CWT method also used the same weight function (W_{ij}) to reduce the uncertainty, thus obtaining the WCWT values.

More detailed descriptions of the backward trajectory, PSCF, and CWT methods can be found in our previous work (Zhang et al., 2018a, 2018b, and 2019a).

3. Results and discussion

3.1. Air pollution episodes during the COVID-19 outbreak

The average concentrations of $PM_{2.5}$, SO_2, NO_2, CO, and O_3 in the BTH region met the 2nd-level air quality during the COVID-19 outbreak due to reduced emissions (GB3095-2012; Fig. 1). The average daily $PM_{2.5}$, SO_2, NO_2, and CO concentrations should be less than 75 μg/m^3, 150 μg/m^3, 80 μg/m^3, and 4 mg/m^3, respectively for 2nd-level air quality in China. No daily standard is proposed for O_3 in China, and the average hourly O_3 concentration should be less than 200 μg/m^3. Despite this, polluted days accounted for 20.8%, 29.9%, and 40.3% of the total number of outbreak days in Beijing, Tianjin, and Shijiazhuang, respectively. In particular, 11.7% of the days during the COVID-19 outbreak were heavily polluted in Shijiazhuang (Fig. 2), thus indicating an urgent need to control air pollution. Therefore, the government faces a considerable challenge to effectively tackle the serious regional air pollution in the BTH region.

The BTH region suffered two large-scale air pollution episodes, one from 23 to 28 January and the other from 8 to 13 February. These were characterized by significantly elevated $PM_{2.5}$, SO_2, NO_2, and CO concentrations. During the first episode, the daily $PM_{2.5}$ concentration in Beijing, Tianjin, and Shijiazhuang was (124.5 ± 47.2) μg/m^3, (157.5 ± 76.0) μg/m^3, and (163.6 ± 24.3) μg/m^3, respectively, with peak hourly values of 204.8 μg/m^3, 281.8 μg/m^3, and 235.1 μg/m^3, respectively. It was also observed that the SO_2, NO_2, and CO concentrations during the first episode increased by 39.0%–136.9%, 5.4%–43.7%, and 90.2–143.0%, respectively, in comparison to periods without pollution episodes in the BTH region. In contrast, the O_3 concentration decreased by 1.5%–8.4% in the BTH region (Fig. 1).

During the second episode, the $PM_{2.5}$ concentration reached (148.4 ± 59.3) μg/m^3, (126.4 ± 27.7) μg/m^3, and (130.9 ± 52.7) μg/m^3 in Beijing, Tianjin, and Shijiazhuang, respectively, which were 1.7–2.0 times higher than the 2nd-level air quality standard in China (24 h average concentration of 75 μg/m^3). The SO_2, NO_2, and CO concentrations during the second episode increased by 16.9%–33.9%, 4.5%–89.5%, and 97.3%–207.0%, respectively, in comparison to periods without pollution episodes in the BTH region (Fig. 1). The O_3 concentration decreased by 16.4% and 33.9% in Beijing and Tianjin, respectively, but increased by 16.6% in Shijiazhuang. Related studies also found that the average O_3 concentration increased during the COVID-19 outbreak compared to 2017–2019 in Hubei Province (Xu et al., 2020), western China (Zhang et al., 2020a), and 366 urban areas across mainland China (Chen et al., 2020b). An increased O_3 concentration is believed to be mainly due to the reduced NO_2 that hinders the reaction between NO and O_3, thus increasing the atmospheric oxidizing capacity (Le et al., 2020; Nichol et al., 2020; Xu et al., 2020). Support for this explanation is provided by the NO_2 concentration in Shijiazhuang, which was 26.8% and 45.5% lower than that in Beijing and Tianjin, respectively, during the second episode. Several studies also reported that NO_x reduction did not significantly avoid air pollution during the COVID-19 outbreak (Tian et al., 2020; Chen et al., 2020a).

These large-scale air pollution episodes were dominated by unfavorable meteorological conditions that comprised a low wind speed and increased relative humidity. The wind speed during the two episodes decreased by 57%, 74%, and 34%, respectively, in Beijing, Tianjin, and Shijiazhuang compared with periods without pollution episodes, while the humidity increased by 50%, 58%, and 23%, respectively (Fig. 3). A stable vertical atmospheric structure weakens the atmospheric turbulent exchange and hinders the diffusion of air pollutants in the vertical direction (Shen et al., 2018; Zhang et al., 2013). There was no significant difference in wind speed between the two heavy pollution periods in Beijing and Tianjin, while the wind speed increased by 41% during the second episode compared with the first episode (Fig. 3). The humidity increased by 22% and 15% in Beijing and Tianjin, respectively during the second episode compared with the first episode, while the decreased by 16% in Shijiazhuang. Therefore, in terms of wind speed and humidity, the meteorological conditions in Beijing and Tianjin during the second episode were more unfavorable to the diffusion of pollutants compared with the first episode, while Shijiazhuang was the opposite. Zheng et al. (2020) found that the sulphate, organic carbon, and secondary inorganic aerosols increased by 2.5%–8.7% in Wuhan city between 23 January and February 22, 2020, thus suggesting the enhanced secondary formation of $PM_{2.5}$ with increased humidity. Chang et al. (2020) reported that the rapid formation of secondary inorganic (mostly nitrate) aerosols was the main factor contributing to air pollution during the COVID-19 outbreak. Our previous results also demonstrated that secondary inorganic aerosols dominated particulate matter (e.g., an average of 48% and 61% in $PM_{2.5}$ and PM_1 (i.e., aerodynamic diameter of <1.0 μm)) and played an essential role during air pollution episodes in Beijing (Liu et al., 2017; Zhang et al., 2018a).

3.2. Backward trajectory analysis during the pollution episodes

The local emission of pollutants and regional pollutant transport both have important impacts on the atmospheric environment. The backward trajectories along with a cluster analysis were conducted to reveal the transport pathways of air masses arriving in the BTH region during the two pollution episodes. A total of 432 trajectories were obtained for each of the three cities (Beijing, Tianjin, and Shijiazhuang) and the abundant trajectories were then divided into four clusters.

3.2.1. Accumulation of local emissions resulting in the first pollution episode

The backward trajectories mainly originated from local emission sources during the first pollution episode in the BTH region. It can be observed that clusters 2, 3, and 1 represented the dominant trajectories in Beijing, Tianjin, and Shijiazhuang, respectively, and corresponded to 58.3%, 51.6%, and 60.6% of the total trajectories

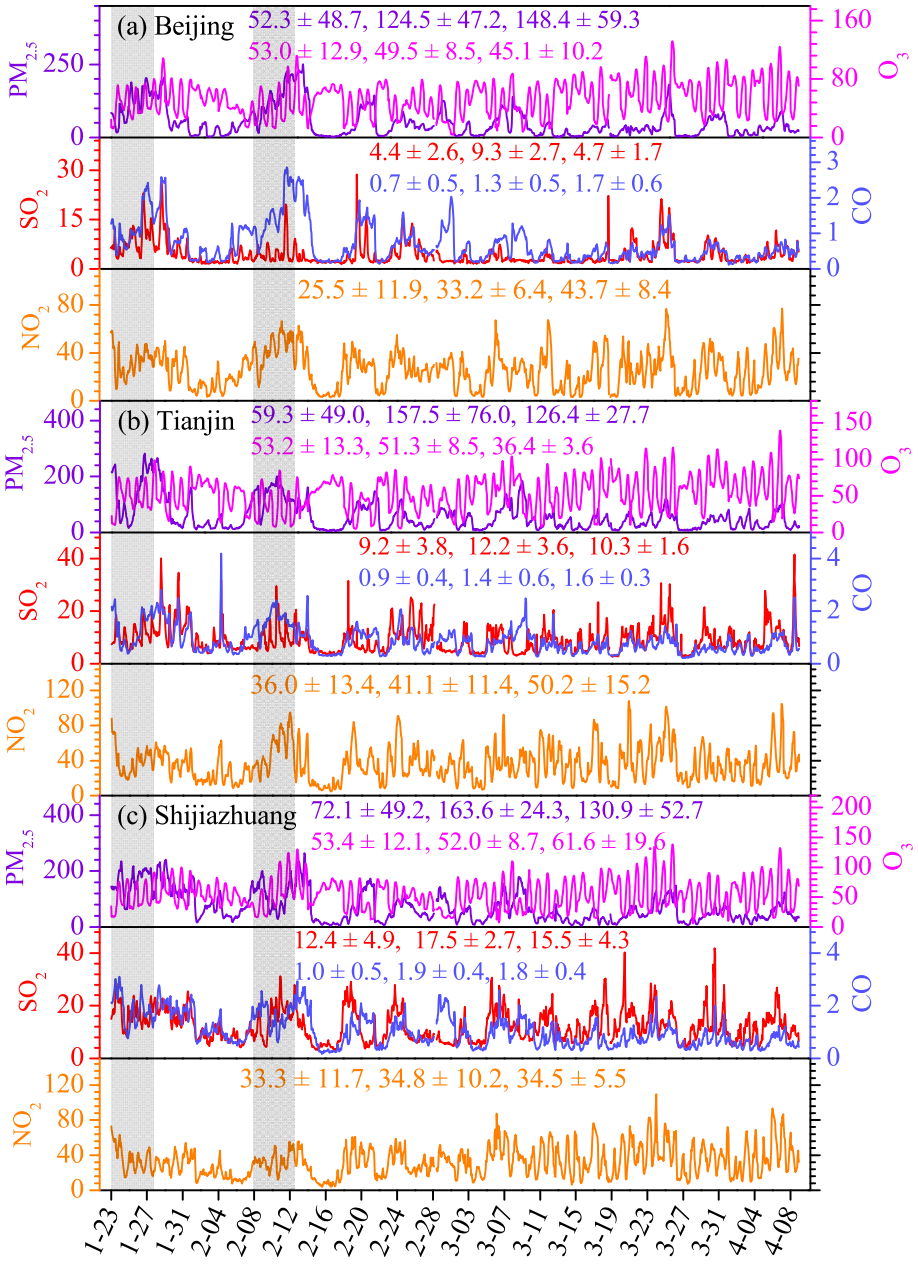

Fig. 1. Time series of air pollutant concentrations during the COVID-19 outbreak in the Beijing–Tianjin–Hebei region.

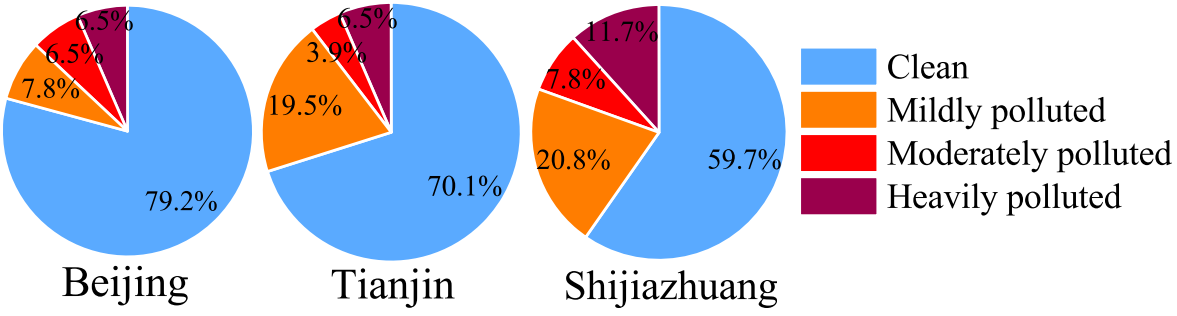

Fig. 2. Proportion of different pollution grades during the COVID-19 outbreak in the Beijing–Tianjin–Hebei region.

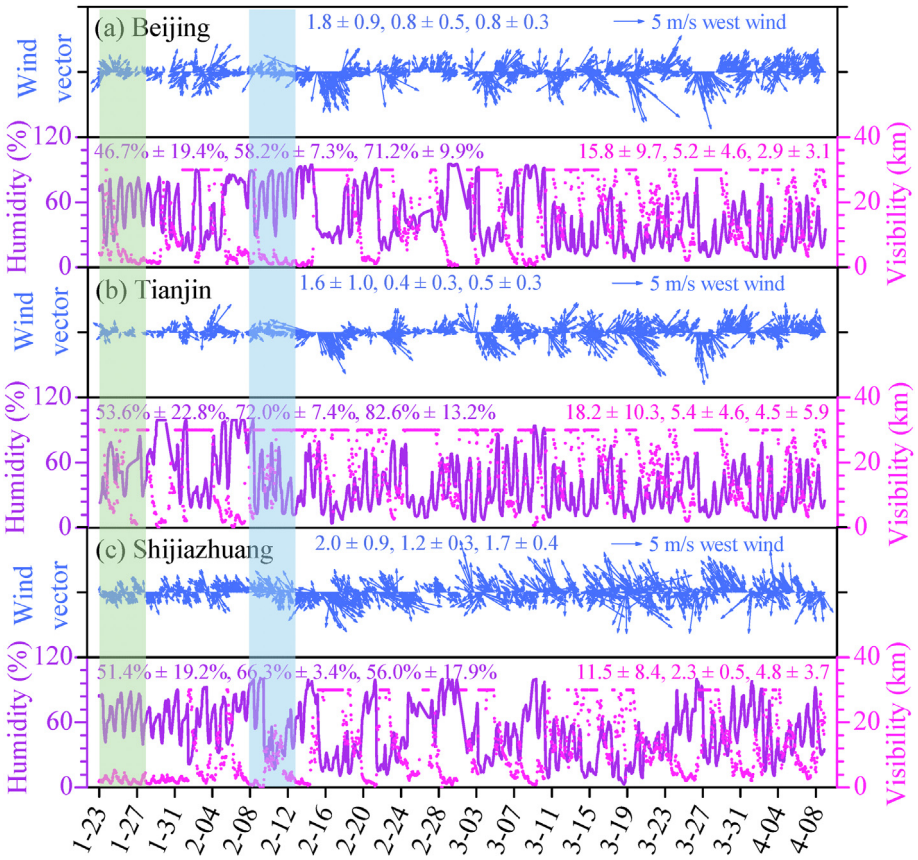

Fig. 3. Time series of meteorological parameters during the COVID-19 outbreak in the Beijing–Tianjin–Hebei region.

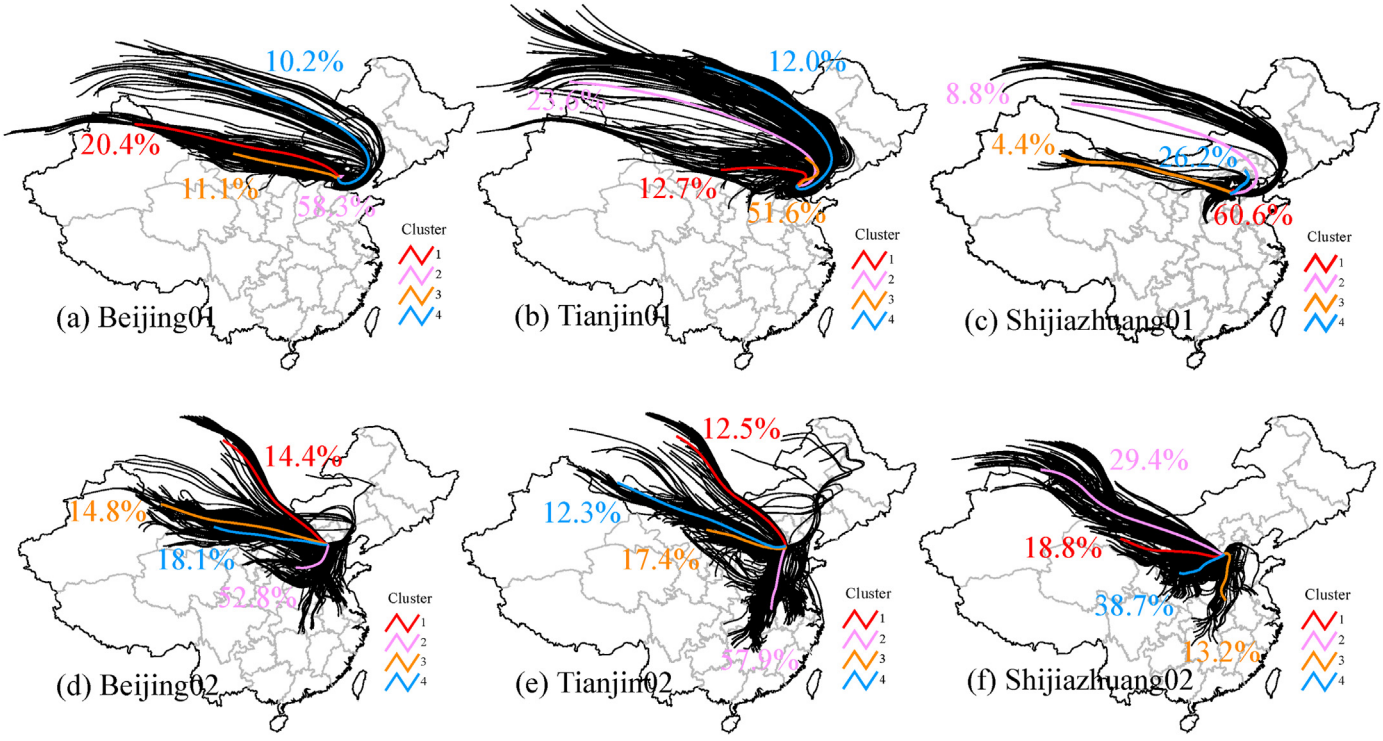

Fig. 4. The 72-h air mass backward trajectories and clusters arriving in the Beijing–Tianjin–Hebei region during the two pollution episodes.

(Fig. 4a–c). The average air pollutant concentrations and meteorological data in each cluster were also calculated to evaluate the impact of individual pathways on air quality in the BTH region (Fig. 5). The dominant clusters in Beijing and Shijiazhuang contained the highest $PM_{2.5}$ concentrations (146.2 μg/m^3 and 173.3 μg/m^3, respectively) as well as high SO_2, CO, and O_3 concentrations. The lowest wind speed and visibility were also found in the dominant clusters, with a wind speed of 0.6 m/s in Beijing and visibility of 2.1–3.0 km in Beijing and Shijiazhuang. The relative humidity reached 61.2% and 64.2% in Beijing and Shijiazhuang, respectively; hence, the conditions were favorable for the secondary formation of $PM_{2.5}$. For Tianjin, cluster 3 from the northeast was dominant (e.g., from Tangshan, a heavily polluted city with an average $PM_{2.5}$ concentration of 160.5 μg/m^3 during this period) and contained the second highest $PM_{2.5}$ concentration of 196.7 μg/m^3. Although cluster 1 from the west contained the highest $PM_{2.5}$ concentration (222.5 μg/m^3), the trajectories only contributed 12.7% of the total trajectories.

The long-distance air mass from the northwest area of the BTH region contributed relatively little to the first pollution episode, with contributions of 30.6%, 35.6%, and 13.2% to the total trajectories for Beijing, Tianjin, and Shijiazhuang, respectively ($PM_{2.5}$ concentrations of 76.2 μg/m^3, 67.2 μg/m^3, and 138.6 μg/m^3). This air mass either primarily originated in western Mongolia and passed thorough eastern Inner Mongolia (e.g., cluster 4 in Beijing, clusters 2 and 4 in Tianjin, and cluster 2 in Shijiazhuang) or in eastern China (e.g., Xinjiang) and passed thorough western Inner Mongolia (e.g., cluster 1 in Beijing and cluster 3 in Shijiazhuang) before arriving in the BTH region.

3.2.2. Short-distance transmission resulting in the second pollution episode

The short-distance air masses from the southern and southwestern areas of the BTH region were the main transport pathways of airflow arriving in the BTH region during the second pollution episode. It can be observed that clusters 2, 2, and 4 represented the dominant trajectories in Beijing, Tianjin, and Shijiazhuang, respectively, contributing 52.8%, 57.9%, and 51.9% to the total trajectories (Fig. 4d–f). For Beijing, the dominant cluster from the southern region (e.g., Baoding, Shijiazhuang, and Taiyuan) contained the highest $PM_{2.5}$ concentration (192.4 μg/m^3). High SO_2, NO_2, CO, and O_3 concentrations, a high humidity, and a low visibility were also associated with the dominant cluster (Fig. 6). Many cities in the southern region of Beijing also experienced serious air pollution during the second pollution episode, especially Baoding and Shijiazhuang, where the air quality reached a severe pollution level (average $PM_{2.5}$ concentration of 176.5 μg/m^3 and 137.2 μg/m^3, respectively). Zhong et al. (2018) reported that the formation of $PM_{2.5}$ pollution in Beijing was primarily caused by pollutants transported from the south of Beijing. Our previous results showed that the average contribution to $PM_{2.5}$ in Beijing from the surrounding regions was 35.4% when the daily $PM_{2.5}$ concentration exceeded 75 μg/m^3 in January of 2010 (Lang et al., 2013).

For Tianjin, cluster 2 from the southern region (e.g., Hebei and Henan provinces) was dominant and contained the lowest $PM_{2.5}$ concentration of 114.0 μg/m^3. Although cluster 4 contained the

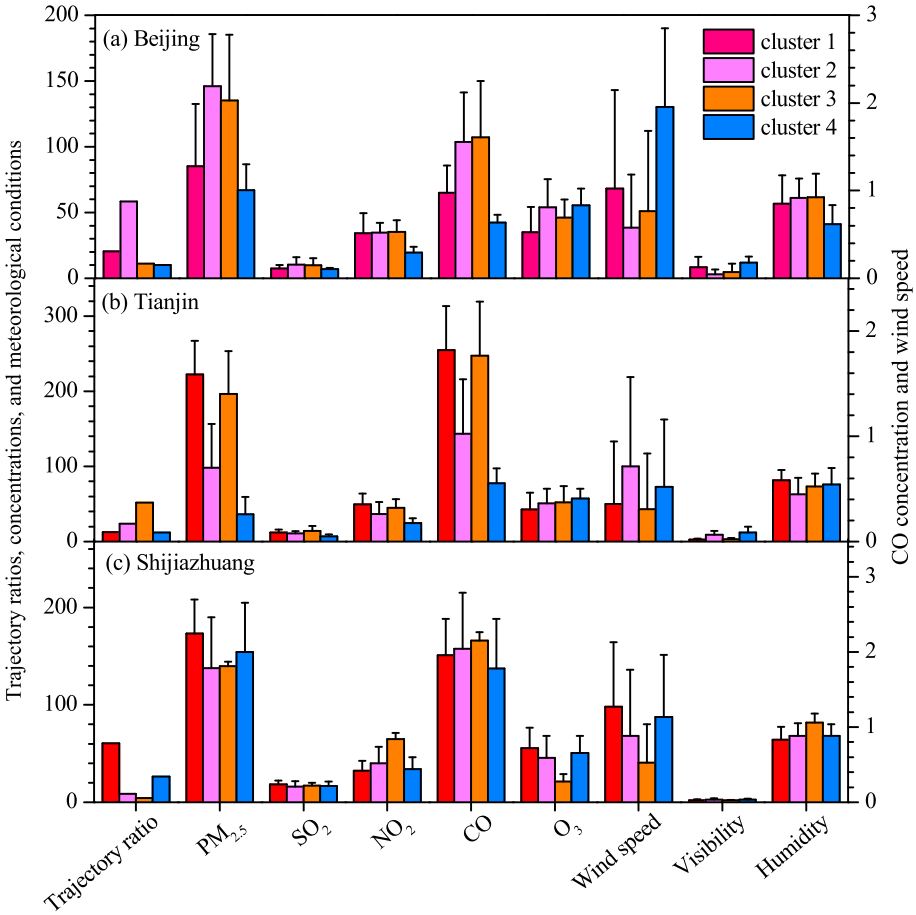

Fig. 5. Trajectory ratios, air pollutant concentrations, and meteorological conditions of each trajectory cluster arriving in the Beijing–Tianjin–Hebei region during the first pollution episode.

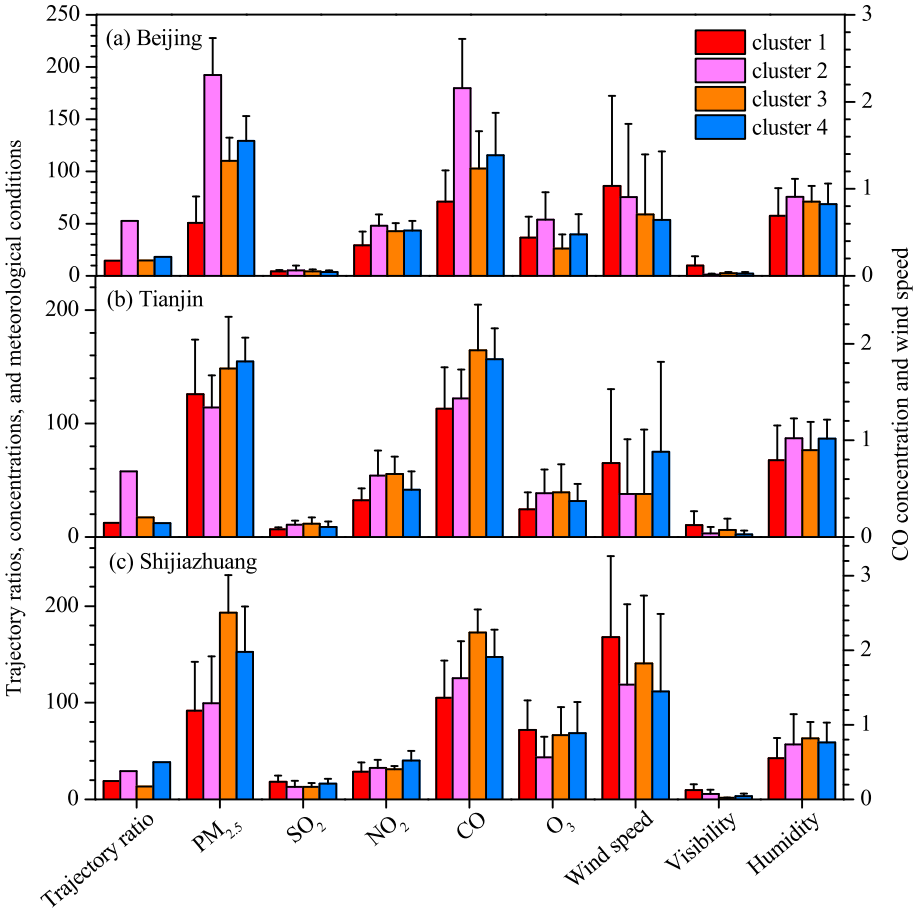

Fig. 6. Trajectory ratios, air pollutant concentrations, and meteorological conditions of each trajectory cluster arriving in the Beijing–Tianjin–Hebei region during the second pollution episode.

highest $PM_{2.5}$ concentration of 154.6 μg/m^3, it only represented 12.3% of the total trajectories. For Shijiazhuang, the dominant cluster was from southwest region (e.g., central Shanxi and Shaanxi provinces) and contained the second highest $PM_{2.5}$ concentration (152.6 μg/m^3). Cluster 3 from the southern region contained the highest $PM_{2.5}$ concentration (193.3 μg/m^3), but trajectories accounted for just 13.2% of the total.

The long-distance air masses (e.g., clusters 1 and 3 in Beijing, clusters 1 and 4 in Tianjin, and cluster 2 in Shijiazhuang) during the second pollution episode also accounted for similar proportions and originated from the northwest of the BTH region, contributing 29.2%, 24.8%, and 29.4% to the total trajectories in Beijing, Tianjin, and Shijiazhuang, respectively. This agrees with the findings during the first episode. The transport pathways of airflow in the BTH region were consistent with the results of Chang et al. (2020), whereby differential transport patterns rather than local emissions may have been responsible for fluctuating aerosol concentrations in Shanghai.

3.3. Potential source regions during the pollution episodes

3.3.1. PSCF analysis

The potential source regions with high WPSCF values (>0.5) were mainly located in the local areas and surrounding regions of Beijing and Shijiazhuang during the first pollution episode (Fig. 7a, c). For Tianjin, apart from the local area, high WPSCF values were also observed in the northeast (e.g., Tangshan City and western Liaoning Province) (Fig. 7b). These observations were generally in good agreements with our backward trajectory analysis as the air pollution was more dominated by local emissions during this period.

During the second pollution episode in Beijing, the potential source regions with high WPSCF values were mainly located in the south-central region of Hebei and western region of Shandong. This finding relates to the various industrial facilities in these areas, which are intensively distributed with a large energy consumption and high air pollutant emissions (Zheng et al., 2019; Zhou et al., 2017, Fig. 7d). This result is consistent with the potential source regions of $PM_{1-2.5}$ in Beijing during the autumn of 2016 (Zhang et al., 2018b), thus proving that air pollutants were transported from locations close to Beijing rather than by long-distance transport. Our previous study showed that the contributions of emissions from Shandong Province and the south-central region of Hebei Province (e.g., Baoding, Cangzhou, Shijiazhuang, Hengshui, Xingtai, and Handan) to the airborne $PM_{2.5}$ in Beijing were 8.1% and 4.3%, respectively, during a pollution episode (Zhang et al., 2019b). For Tianjin, the potential source regions with high WPSCF values were primarily located in the southern region (e.g., Shijiazhuang, Handan, Xingtai, and Zhengzhou), which agrees with the dominance of cluster 2 (Fig. 7e). Besides, high WPSCF values were also found in the western and northwest areas of Tianjin. These were situated along the pathway of dominant clusters 1, 3, and 4, which exhibited higher $PM_{2.5}$ concentrations (125.8–154.6 μg/m^3) compared with cluster 2 in the southern region. For Shijiazhuang,

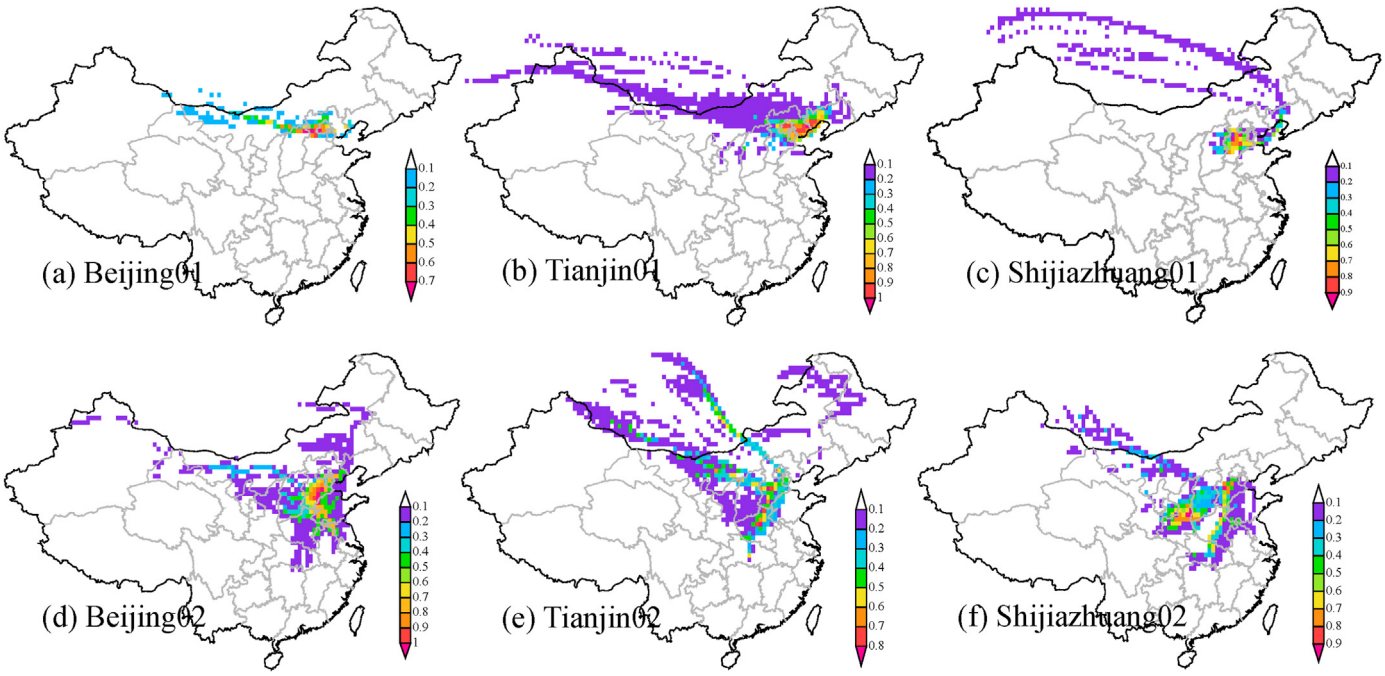

Fig. 7. Weighted potential source contribution function (WPSCF) maps for $PM_{2.5}$ arriving in the Beijing–Tianjin–Hebei region during the two pollution episodes.

the potential source regions with high WPSCF values were concentrated in the central region of Shaanxi Province and in the southern region of Shijiazhuang, which was consistent with the results for Tianjin (Fig. 7f).

3.3.2. CWT analysis

The potential source regions with higher WCWT values generally agreed with the results of the WPSCF during the first pollution episode (Fig. 8a–c). However, the results of WCWT differed to the WPSCF results in some aspects in Beijing, whereby high WCWT values were also found in Tangshan. In addition, the regions with lower WCWT values indicate that $PM_{2.5}$ pollution in the BTH region was unaffected by long-distance transport from eastern Inner Mongolia and eastern China during this episode.

During the second pollution episode, the potential source regions with higher WCWT values were consistent with the results of the trajectory cluster and WPSCF in Beijing, whereas they covered a wider range than the WPSCF results for Tianjin and Shijiazhuang

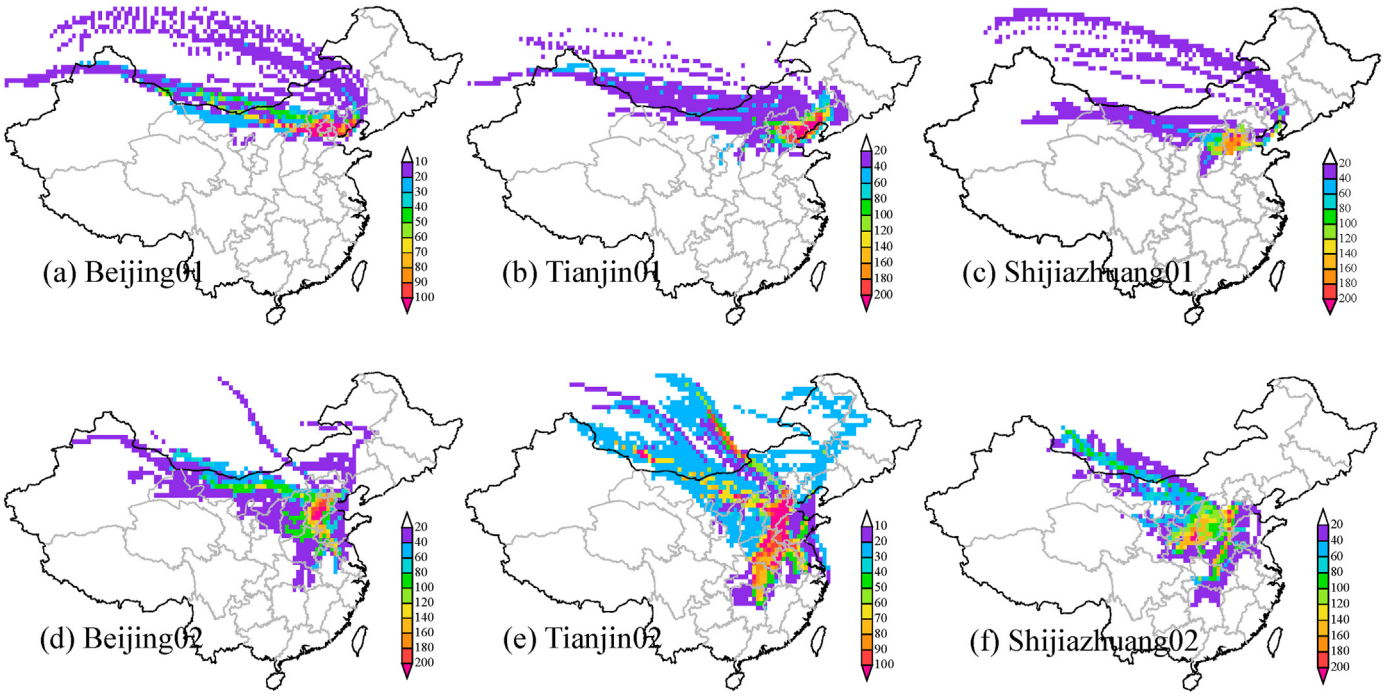

Fig. 8. Weighted concentration weighted trajectory (WCWT) maps for $PM_{2.5}$ arriving in the Beijing–Tianjin–Hebei region during the two pollution episodes.

(Fig. 8d–f). For example, in Tianjin, the potential source regions were located in the south-central region of Hebei Province and western region of Shandong Province (WCWT of >100 μg/m^3) as well as Henan Province and eastern Hubei Province. For Shijiazhuang, the potential source regions were located in the southwest region (e.g., Shanxi and central Shaanxi provinces) and southern region. The high probabilities and levels of the WCWT observed in southern, southwest, and northwest regions of the BTH region during the second pollution episode further confirmed that regional pollution transport in addition to local emissions may have influenced the air quality.

3.4. Comparison with other studies

Although the source distribution of air pollution during the COVID-19 outbreak in the BTH region has not been reported elsewhere to date, several studies have analyzed the source distribution in this region during other periods (Table 1), which can be compared with the results obtained here.

Zhang et al. (2015) reported that the potential sources for Beijing during the winter of 2013 were mainly located in Beijing itself and in the surrounding regions with a WPSCF value of >0.7, which is consistent with our results for Beijing during the first pollution episode. On the contrary, both Wang et al. (2015b) and Li et al. (2017a) found that the clusters from the north and northwest of Beijing were prevailing during the winter and contributed 75%–95%, whereas we determined contributions of just 41.7%–47.2% for Beijing during the two pollution episodes. We note that Wang et al. (2015b) and Li et al. (2017a) reported an average $PM_{2.5}$ concentration of 74 μg/m^3 and 82 μg/m^3, respectively, which are considerably lower than that during the two pollution episodes in our study (124.5–148.4 μg/m^3). We speculate that the contribution of air masses from the southern area of Beijing might have increased during the air pollution episodes. The results of the PSCF analysis indicate that the major potential sources were mainly focused in southern, western, and eastern Hebei Province, and north-western Shandong Province (WPSCF of >0.5) (Wang et al., 2015b). This is in general agreement with our results for Beijing during the second pollution episode (south-central Hebei and western Shandong provinces). Li et al. (2017a) also found potential sources in central Inner Mongolia corresponding to a WPSCF of >0.8. Qiao et al. (2017) reported that the airflow from southern Hebei Province and western Shandong Province exerted the most significant external influence on the air quality in Beijing during the 2008 Olympics, which was generally consistent with our results for Beijing during the second pollution episode. However, the dominant clusters in Qiao et al. (2017) were from the southeast, northwest, and southern areas of Beijing, which contributed 23%, 23%, and 21% to the total trajectories; thus, these results differ to our study as we found that they were mainly from the southern region (52.8%) during the second pollution episode. Dong et al. (2020) determined that the potential source regions with high WPSCF values were primarily located in northern and central Shanxi Province, which is the largest coal production area in China.

Zhao et al. (2019) analyzed the transport pathways and potential source regions in Tianjin during two pollution episodes in 2018. The dominant trajectories were from the southern region and contributed 49%–76% of the total trajectories, which agrees with our results during the second episode (57.9%). Zhao et al. (2019) also found that the southern region contributed the most to the level of $PM_{2.5}$, with the PSCF value exceeding 0.9 during the two pollution episodes. Higher PSCF values were also observed in southern Mongolia, which is consistent with our results for the second pollution episode. Lv (2019) reported that the clusters from Inner Mongolia, Shaanxi, and Shanxi contributed 41%, which agrees with our results for Shijiazhuang during the first pollution episode (39.4%). Liu et al. (2019) also determined the potential source regions of $PM_{2.5}$ in Tianjin and Shijiazhuang during a winter pollution episode in 2017, although the regional coverage was not wider than our results.

The results of these studies evidence that pollution transport pathways and potential source regions are influenced by geographical location and local climate, thus indicating the importance of the present study of the BTH region during the COVID-19 outbreak to explore the source distribution.

4. Conclusion

Improving our understanding of the transport pathways and potential source regions of air pollution is critical for the development and implementation of pollution control policy. Although air quality in the BTH region was effectively improved during the COVID-19 lockdown in China, two large-scale air pollution episodes did occur from 23 to January 28, 2020 and from 8 to February 13,

Table 1
Source distribution of air pollution in the Beijing-Tianjin-Hebei region during other periods.

Study area	Period	Dominant trajectory (contribution)	Potential source regions	Literature
Beijing	Winter 2013	–	Local area and Hebei	Zhang et al., (2015)
Beijing	Winter 2005–2010	North and northwest of Beijing (95%)	Southern, western, and eastern Hebei, and north-western Shandong	Wang et al., (2015b)
Beijing	Winter 2014, 2015	Northwest of Beijing (75%)	Southern Hebei, northern Shanxi, western Shandong, and central Inner Mongolia	Li et al., (2017a)
Beijing[a]	June and October 2008 covered by the Olympic Games	Southeast of Beijing (23%) Northwest of Beijing (23%) Southern of Beijing (21%)	Southern Hebei, western Shandong	Qiao et al., (2017)
Beijing	December 2017 to December 2018	–	Northern and central Shanxi	Dong et al., (2020)
Tianjin	Pollution episode during March 9–17, 2018	Eastern Hebei, western Shandong, eastern Henan, and eastern Hubei (76%)	Consistent with the dominant trajectory	Zhao et al., (2019)
	Pollution episode during November 22–30, 2018	Eastern Hebei (49%)	Southern Hebei, western Shandong, and southern Mongolia	
Tianjin	Pollution episode during winter 2017	–	Southern Tianjin, central and southern Hebei, northern Shandong, and northern Henan	Liu et al., (2019)
Shijiazhuang			Southern Hebei and central Shanxi	
Shijiazhuang	Pollution episodes 2011–2018	Inner Mongolia, Shaanxi, and Shanxi (41%)	–	Lv, (2019)

[a] The results of PM_{10}. — indicates not reported.

2020. These were characterized by significantly elevated $PM_{2.5}$, SO_2, NO_2, and CO concentrations as a result of the unfavorable meteorological conditions during these periods. The wind speed during these two episodes decreased by 34%–74% in comparison to period without pollution episodes, while the humidity increased by 23%–58%. Meteorological conditions should be considered when setting control strategies and air quality goals. Although anthropogenic emissions reduced significantly during the COVID-19 lockdown, the O_3 concentration increased during the second pollution episode in Shijiazhuang. A synergistic control including a reduction in the NO_x/VOCs ratio is required to reduce the O_3 concentration because a high ratio was most likely responsible for the increased O_3 concentration. Local pollutant emissions and regional pollutant transport have important impacts on the atmospheric environment. The air pollution in the BTH region was mainly affected by local emission sources during the first episode, whereas the second episode was affected by short-distance air masses that originated from Hebei, Henan, central Shanxi, and Shaanxi provinces. Thus it can be seen that the emission reduction of anthropogenic sources cannot completely offset the impact of unfavorable meteorological conditions on air quality. Therefore, on the basis of local emission reduction, enhancing regional environmental cooperation and implementing a united prevention and control of air pollution are effective mitigation measures for the BTH region.

Author contribution

Na Zhao: Conceptualization, Methodology, Investigation, Resources, Writing - original draft, Writing - review & editing. Gang Wang: Conceptualization, Methodology, Writing - original draft, Writing - review & editing, Supervision. Guohao Li: Conceptualization, Methodology, Writing - review & editing. Jianlei Lang: Conceptualization, Methodology, Writing - review & editing, Supervision. Hanyu Zhang: Methodology, Resources, Writing - review & editing.

Declaration of competing interest

The authors declare that they have no known competing financial interests or personal relationships that could have appeared to influence the work reported in this paper.

Acknowledgements

This work was supported by the National Science Foundation of China (21806086 & 51878012), the Fundamental Research Funds for the Central Universities (20CX06008A) and the Beijing Nova Program (Z201100006820098) from Beijing Municipal Science & Technology Commission.

Appendix A. Supplementary data

Supplementary data to this article can be found online at https://doi.org/10.1016/j.envpol.2020.115617.

References

Chang, Y., Huang, R., Ge, X., Huang, X., Hu, J., Duan, Y., Zou, Z., Liu, X., Lehmann, M.F., 2020. Puzzling haze events in China during the coronavirus (COVID-19) shutdown. Geophys. Res. Lett. 47, e2020GL088533 https://doi.org/10.1029/2020gl088533.

Chen, H., Huo, J., Fu, Q., Duan, Y., Xiao, H., Chen, J., 2020a. Impact of quarantine measures on chemical compositions of $PM_{2.5}$ during the COVID-19 epidemic in Shanghai, China. Sci. Total Environ. 743, 140758. https://doi.org/10.1016/j.scitotenv.2020.140758.

Chen, Q.X., Huang, C.L., Yuan, Y., Tan, H.P., 2020b. Influence of COVID-19 event on air quality and their association in mainland China. Aerosol Air Qual. Res. 20, 1541–1551. https://doi.org/10.4209/aaqr.2020.05.0224.

Cheng, M.D., Hopke, P.K., Barrie, L., Rippe, A., Olson, M., Landsberger, S., 1993. Qualitative determination of source regions of aerosol in Canadian high arctic. Environ. Sci. Technol. 27, 2063–2071. https://doi.org/10.1021/es00047a011.

Chu, B., Zhang, S., Liu, J., Ma, Q., He, H., 2020. Significant concurrent decrease in $PM_{2.5}$ and NO_2 concentrations in China during COVID-19 epidemic. J. Environ. Sci. https://doi.org/10.1016/j.jes.2020.06.031.

Ding, X., Kong, L., Du, C., Zhanzakova, A., Wang, L., Fu, H., Chen, J., Yang, X., Cheng, T., 2017. Long-range and regional transported size-resolved atmospheric aerosols during summertime in urban Shanghai. Sci. Total Environ. 583, 334–343. https://doi.org/10.1016/j.scitotenv.2017.01.073.

Dong, G., Tang, G., Zhang, J., Liu, Q., Yan, G., Cheng, M., Gao, W., Wang, Y., Wang, Y., 2020. Characteristics of carbonaceous species in $PM_{2.5}$ in southern Beijing (in Chinese). Environ. Sci. https://doi.org/10.13227/j.hjkx.202003031.

Faridi, S., Yousefian, F., Niazi, S., Ghalhari, M.R., Hassanvand, M.S., Naddafi, K., 2020. Impact of SARS-CoV-2 on ambient air particulate matter in Tehran. Aerosol Air Qual. Res. https://doi.org/10.4209/aaqr.2020.05.0225.

Geng, G.N., Xiao, Q.Y., Zheng, Y.X., Tong, D., Zhang, Y.X., Zhang, X.Y., Zhang, Q., He, K.B., Liu, Y., 2019. Impact of China's air pollution prevention and control action plan on $PM_{2.5}$ chemical composition over eastern China. Sci. China Earth Sci. 62, 1872–1884. https://doi.org/10.1007/s11430-018-9353-x.

Hui, L., Liu, X., Tan, Q., Feng, M., An, J., Qu, Y., Zhang, Y., Cheng, N., 2019. VOC characteristics, sources and contributions to SOA formation during haze events in Wuhan, central China. Sci. Total Environ. 650, 2624–2639. https://doi.org/10.1016/j.scitotenv.2018.10.029.

John, K., Karnae, S., Crist, K., Kim, M., Kulkarni, A., 2012. Analysis of trace elements and ions in ambient fine particulate matter at three elementary schools in Ohio. J. Air Waste Manag. Assoc. 57, 394–406. https://doi.org/10.3155/1047-3289.57.4.394.

Lang, J., Cheng, S., Li, J., Chen, D., Zhou, Y., Wei, X., Han, L., Wang, H., 2013. A monitoring and modeling study to investigate regional transport and characteristics of $PM_{2.5}$ pollution. Aerosol Air Qual. Res. 13, 943–956. https://doi.org/10.4209/aaqr.2012.09.0242.

Lang, J., Cheng, S., Wei, W., Zhou, Y., Wei, X., Chen, D., 2012. A study on the trends of vehicular emissions in the Beijing-Tianjin-Hebei (BTH) region, China. Atmos. Environ. 62, 605–614. https://doi.org/10.1016/j.atmosenv.2012.09.006.

Le, T., Wang, Y., Liu, L., Yang, J., Yung, Y., Li, G., Seinfeld, J., 2020. Unexpected air pollution with marked emission reductions during the COVID-19 outbreak in China. Science. https://doi.org/10.1126/science.abb7431.

Li, D., Liu, J., Zhang, J., Gui, H., Du, P., Yu, T., Wang, J., Lu, Y., Liu, W., Cheng, Y., 2017a. Identification of Long-Range Transport Pathways and Potential Sources of $PM_{2.5}$ and PM_{10} in Beijing from 2014 to 2015, vol. 56, pp. 214–229. https://doi.org/10.1016/j.jes.2016.06.035.

Li, L., Yan, D., Xu, S., Huang, M., Wang, X., Xie, S., 2017b. Characteristics and source distribution of air pollution in winter in Qingdao, eastern China. Environ. Pollut. 224, 44–53. https://doi.org/10.1016/j.envpol.2016.12.037.

Liu, C., Hua, C., Zhang, H., Zhang, B., Wang, G., Zhu, W., Xu, R., 2019. A severe fog-haze episode in Beijing-Tianjin-Hebei region: characteristics, sources and impacts of boundary layer structure. Atmos Pollut Res 10, 1190–1202. https://doi.org/10.1016/j.apr.2019.02.002.

Liu, H., Liu, C., Xie, Z., Li, Y., Huang, X., Wang, S., Xu, J., Xie, P., 2016. A paradox for air pollution controlling in China revealed by "APEC Blue" and "Parade Blue". Sci. Rep. 6, 34408. https://doi.org/10.1038/srep34408.

Liu, X., Lang, J., Cheng, S., Wang, X., Wang, G., 2017. Pollution characteristics and regional migration impact of $PM_{2.5}$ in Beijing in winter season (in Chinese). J. Saf. Environ. 17, 1200–1205. https://doi.org/10.13637/j.issn.1009-6094.2017.03.072.

Lv, Z., 2019. Chemical Characteristics and Source Apportionment of Water-Soluble Ions in PM2.5 in Shijiazhuang (In Chinese). Master's thesis. East China University of Technology, Nanchang, China.

Ministry of ecology and environment of the people's republic of China (MEE). Bulletin of China's ecological environment in 2019 (in Chinese), 2 June. http://www.mee.gov.cn/hjzl/sthjzk/.

Navinya, C., Patidar, G., Phuleria, H.C., 2020. Examining effects of the COVID-19 national lockdown on ambient air quality across urban India. Aerosol Air Qual. Res. https://doi.org/10.4209/aaqr.2020.05.0256.

Nichol, J., Bilal, M., Ali, M., Qiu, Z., 2020. Air pollution scenario over China during COVID-19. Rem. Sens. 12, 2100. https://doi.org/10.3390/rs12132100.

Qiao, Q., Huang, B., Piper, J.D.A., Biggin, A.J., Zhang, C., 2017. The characteristics of environmental particulate matter in the urban area of Beijing, China, during the 2008 Olympic Games. Atmos Pollut Res 8, 141–148. https://doi.org/10.1016/j.apr.2016.08.003.

Shen, Y., Zhang, L.P., Fang, X., Ji, H.Y., Li, X., Zhao, Z.W., 2018. Spatiotemporal patterns of recent $PM_{2.5}$ concentrations over typical urban agglomerations in China. Sci. Total Environ. 655, 13–26. https://doi.org/10.1016/j.scitotenv.2018.11.105.

Tian, H., Liu, Y., Li, Y., Wu, C., Chen, B., Kraemer, M., Li, B., Cai, J., Xu, B., Yang, Q., Wang, B., Yang, P., Cui, Y., Song, Y., Zheng, P., Wang, Q., Bjornstad, O., Yang, R., Grenfell, B., Pybus, O., Dye, C., 2020. An investigation of transmission control measures during the first 50 days of the COVID-19 epidemic in China. Science 368, 638–642. https://doi.org/10.1126/science.abb6105.

Wang, G., Cheng, S., Li, J., Lang, J., Wen, W., Yang, X., Tian, L., 2015a. Source apportionment and seasonal variation of $PM_{2.5}$ carbonaceous aerosol in the Beijing-Tianjin-Hebei Region of China. Environ. Monit. Assess. 187 https://doi.org/10.1007/s10661-015-4288-x.

Wang, G., Cheng, S., Wei, W., Yang, X., Wang, X., Jia, J., Lang, J.L., Lv, Z., 2017.

Characteristics and emission-reduction measures evaluation of $PM_{2.5}$ during the two major events: APEC and Parade. Sci. Total Environ. 595, 81–92. https://doi.org/10.1016/j.scitotenv.2017.03.231.

Wang, L., Liu, Z., Sun, Y., Ji, D., Wang, Y., 2015b. Long-range transport and regional sources of $PM_{2.5}$ in Beijing based on long-term observations from 2005 to 2010. Atmos. Res. 157, 37–48. https://doi.org/10.1016/j.atmosres.2014.12.003.

Wang, P.F., Chen, K.Y., Zhu, S.Q., Wang, P., Zhang, H.L., 2020. Severe air pollution events not avoided by reduced anthropogenic activities during COVID-19 outbreak. Resour. Conserv. Recycl. 158, 104814. https://doi.org/10.1016/j.resconrec.2020.104814.

Wang, S., Zhao, M., Xing, J., Ye, W., Zhou, Y., Lei, Y., He, K., Fu, L., Hao, J., 2010. Quantifying the air pollutants emission reduction during the 2008 Olympic Games in Beijing. Environ. Sci. Technol. 44, 2490–2496. https://doi.org/10.1021/es9028167.

Wang, Y., Li, W., Gao, W., Liu, Z., Tian, S., Shen, R., Ji, D., Wang, S., Wang, L., Tang, G., Song, T., Cheng, M., Wang, G., Gong, Z., Hao, J., Zhang, Y., 2019. Trends in particulate matter and its chemical compositions in China from 2013-2017. Sci. China Earth Sci. 62, 1857–2187. https://doi.org/10.1007/s11430-018-9373-1.

Xiong, Y., Du, K., 2020. Source-resolved attribution of ground-level ozone formation potential from VOC emissions in Metropolitan Vancouver, BC. Sci. Total Environ. 721, 137698. https://doi.org/10.1016/j.scitotenv.2020.137698.

Xu, K., Cui, K., Young, L.H., Hsieh, Y.K., Wang, Y.F., Zhang, J., Wan, S., 2020. Impact of the COVID-19 event on air quality in central China. Aerosol Air Qual. Res. 20, 915–929. https://doi.org/10.4209/aaqr.2020.04.0150.

Zhang, H., Cheng, S., Wang, X., Yao, S., Zhu, F., 2018a. Continuous monitoring, compositions analysis and the implication of regional transport for submicron and fine aerosols in Beijing, China. Atmos. Environ. 195, 30–45. https://doi.org/10.1016/j.atmosenv.2018.09.043.

Zhang, H., Cheng, S., Yao, S., Wang, X., Zhang, J., 2019a. Pollution characteristics and regional transport of atmospheric particulate matter in Beijing from October to November, 2016 (in Chinese). Environ. Sci. 40, 1999–2009. https://doi.org/10.13227/j.hjkx.201810228.

Zhang, H., Cheng, S., Yao, S., Wang, X., Zhang, J., 2019b. Multiple perspectives for modeling regional $PM_{2.5}$ transport across cities in the Beijing-Tianjin-Hebei region during haze episodes. Atmos. Environ. 212, 22–35. https://doi.org/10.1016/j.atmosenv.2019.05.031.

Zhang, J., Cui, K., Wang, Y.F., Wu, J.L., Huang, W.S., Wan, S., Xu, K., 2020a. Temporal variations in the air quality index and the impact of the COVID-19 event on air quality in western China. Aerosol Air Qual. Res. 20, 1552–1568. https://doi.org/10.4209/aaqr.2020.06.0297.

Zhang, R.X., Zhang, Y.Z., Lin, H.P., Feng, X., Fu, T.M., Wang, Y.H., 2020b. NOx emission reduction and recovery during COVID-19 in East China. Atmosphere 11, 433. https://doi.org/10.3390/atmos11040433.

Zhang, X., Sun, J., Wang, Y., Li, W., Zhang, Q., 2013. Factors contributing to haze and fog in China. Chin. Sci. Bull. 58, 1178–1187. https://doi.org/10.1360/972013-150.

Zhang, Y., Lang, J.L., Cheng, S., Li, S., Zhou, Y., Chen, D., Zhang, H., Wang, H., 2018b. Chemical composition and sources of PM1 and $PM_{2.5}$ in Beijing in autumn. Sci. Total Environ. 630, 72–82. https://doi.org/10.1016/j.scitotenv.2018.02.151.

Zhang, Z., Wong, M., Lee, K., 2015. Estimation of potential source regions of $PM_{2.5}$ in Beijing using backward trajectories. Atmos Pollut Res 6, 173–177. https://doi.org/10.5094/APR.2015.020.

Zhao, H., Wu, Z., Liu, J., Wu, G., 2019. Two air pollution events in the coastal city of Tianjin, north China plain. Atmos Pollut Res 10, 1780–1794. https://doi.org/10.1016/j.apr.2019.07.009.

Zheng, H., Cai, S., Wang, S., Zhao, B., Chang, X., Hao, J., 2019. Development of a unit-based industrial emission inventory in the Beijing-Tianjin-Hebei region and resulting improvement in air quality modeling. Atmos. Chem. Phys. 19, 3447–3462. https://doi.org/10.5194/acp-19-3447-2019.

Zheng, H., Kong, S., Chen, N., Yan, Y., Liu, D., Zhu, B., Xu, K., Cao, W., Ding, Q., Lan, B., Zhang, Z., Zheng, M., Fan, Z., Cheng, Y., Zheng, S., Yao, L., Bai, Y., Zhao, T., Qi, S., 2020. Significant changes in the chemical compositions and sources of $PM_{2.5}$ in Wuhan since the city lockdown as COVID-19. Sci. Total Environ. 739, 140000 https://doi.org/10.1016/j.scitotenv.2020.140000.

Zhong, J., Zhang, X., Dong, Y., Wang, Y., Liu, C., Wang, J., Zhang, Y., Che, H., 2018. Feedback effects of boundary-layer meteorological factors on cumulative explosive growth of $PM_{2.5}$ during winter heavy pollution episodes in Beijing from 2013 to 2016. Atmos. Chem. Phys. 18, 247–258. https://doi.org/10.5194/acp-18-247-2018.

Zhou, Y., Xing, X., Lang, J., Chen, D., Cheng, S., Wei, L., Wei, X., Liu, C., 2017. A comprehensive biomass burning emission inventory with high spatial and temporal resolution in China. Atmos. Chem. Phys. 17, 2839–2864.